Deposition, Characterization, and Thin-Film-Based Chemical Sensing of Ultra-Long Chemically Synthesized Graphene Nanoribbons

Ahmad N. Abbas [‡,ϒ,□], Gang Liu [‡,□], Akimitsu Narita[†], Manuel Orosco[¶], Xinliang Feng[†], Klaus Müllen[†] and Chongwu Zhou [‡*]

‡ Department of Electrical Engineering, University of Southern California, Los Angeles, California 90089, United States

† Max Planck Institute of Polymer Research, Ackermannweg 10, 55128 Mainz, Germany

¶ Alfred E. Mann institute for Biomedical Engineering, University of Southern California, Los Angeles, California 90089, United States

ϒ Department of Electrical Engineering, King Abdulaziz University, Abdullah Sulayman St, Jeddah 22254, Saudi Arabia

□ Equal Contributions

Supporting Information

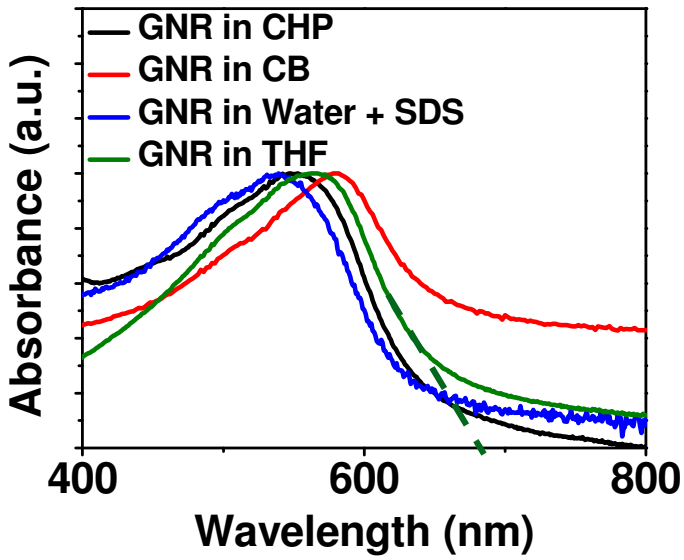

Figure s1. ultraviolet-visible (UV-vis) absorption spectrum of GNR **1a** dissolved in 1-cyclohexyl-2-pyrrolidone (CHP), chlorobenzene (CB) and tetrahydrofuran (THF). Notably, GNR **1b** could be dispersed in deionized water with sodium dodecyl sulfate (SDS), where GNR **1a** showed no dispersibility. Absorption peak position of ~540 - 580 nm was observed with the slight peak position variance attributed to different levels of GNRs aggregation in different solvents and the interaction of SDS with GNR. Moreover, the optical bandgap of the GNRs can be extrapolated from the x-intercept of the UV-vis spectrum in Figure 1b (dashed green line) which yields a value of ~1.84 eV.

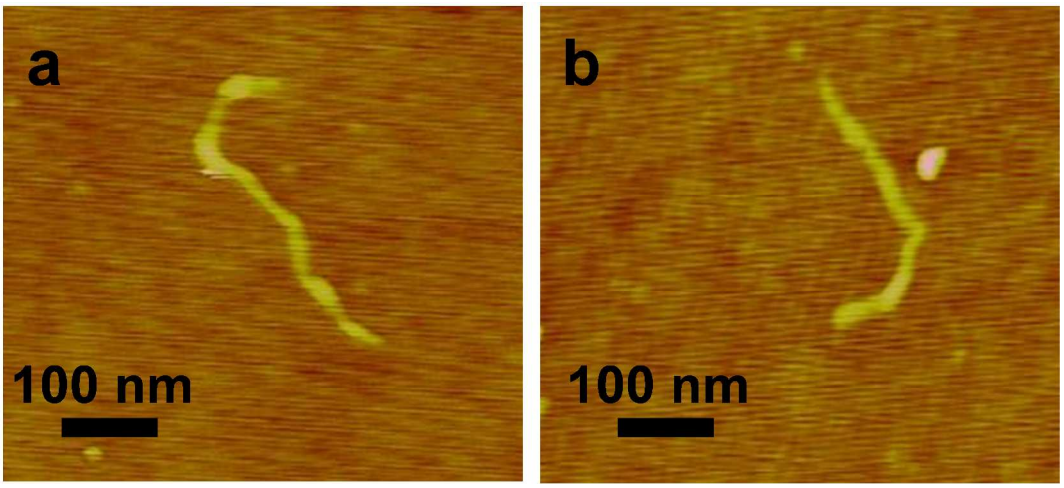

Figure s2. AFM images of typical individual GNRs on dodecyltriethoxysilane functionalized SiO_2 surface showing lengths of 300 to 500 nm.

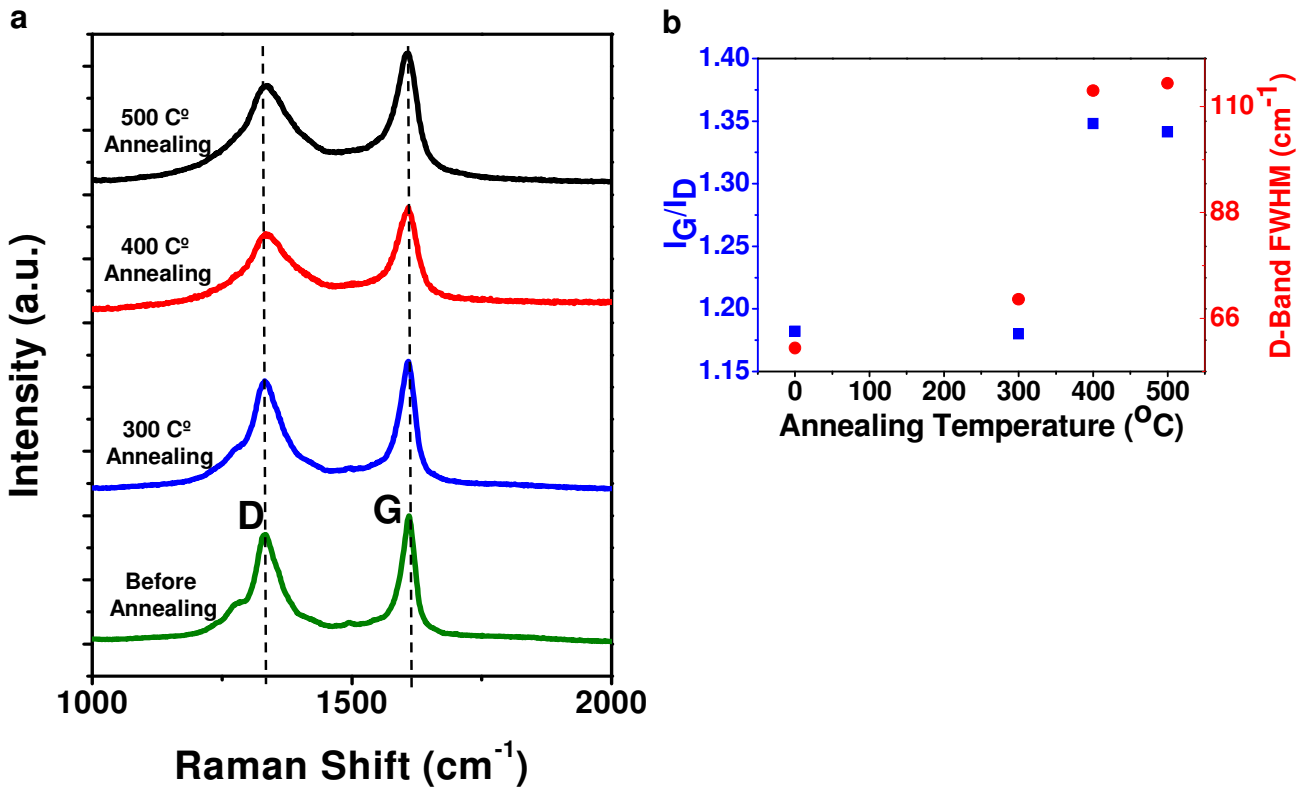

Figure s3. a) Raman spectra of a GNR film before annealing and after sequential annealing at 300 °C, 400 °C, and 500 °C. b) I_G/I_D ratio (blue squares) and D-band full width half maximum (FWHM) of GNR films (red circles) *vs.* annealing temperatures. The I_G/I_D ratio even showed a slight increase at annealing temperatures of 400 and 500 °C compared to pristine GNR and GNR after annealing at 300 °C, which indicates that the annealing samples at conditions we used does not affect the GNR basal plane, as otherwise I_G/I_D would decrease due to defect formation. While we do not have a clear understanding of the cause of D-band broadening, we hypothesize that broadening of the D-band peak upon annealing might be derived from the removal of the alkyl chains and/or covalent bond formation between neighboring GNRs at the high temperatures.

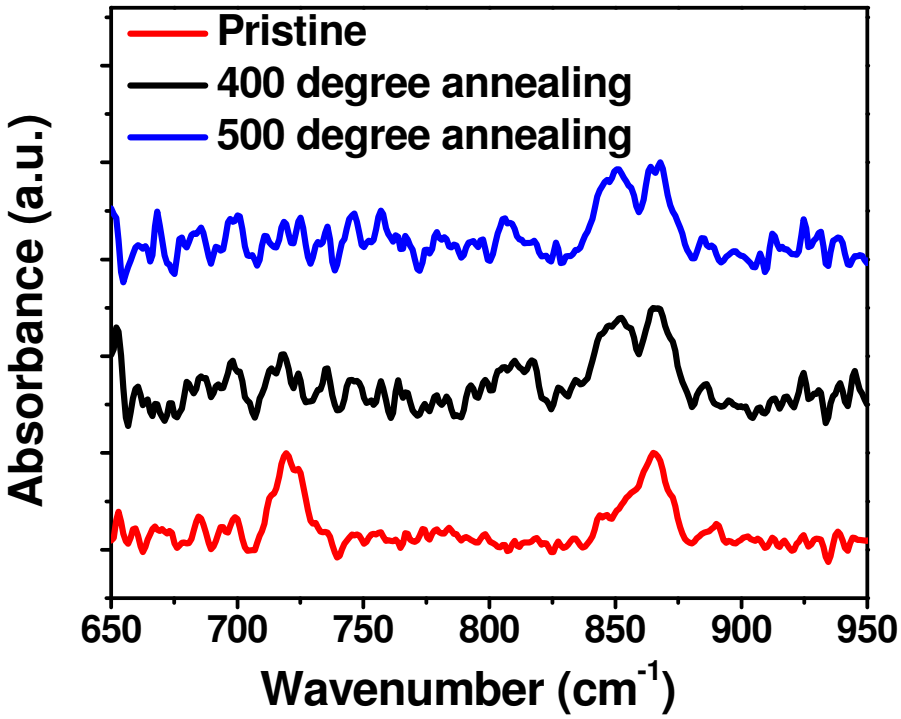

Figure s4. ATR-FTIR spectra of pristine, 400 °C and 500 °C annealed GNR films showing the disappearance of peak at ~720 cm^{-1} associated with alkyl chains. The peak at ~862 cm^{-1} represents the C-H bond at the cove position and is unaffected by annealing. We hypothesize that the additional peak at ~850 cm^{-1} might correspond to similar C-H bond at the cove position of GNRs after removal of the alkyl chains or covalent bond formation with neighboring GNRs.

Note s1:

Experimental Methods:

Individual GNR deposition: The GNR dispersion is prepared by sonicating GNR powder in 1-cyclohexyl-2-pyrrolidone (CHP) for 30 min to 1 h in a glass vial. Then, the dispersion is centrifuged at 1500 rpm for 5 min. The SiO_2 surface is functionalized by incubating the substrate in (1:10) (dodecyltriethoxysilane : isopropyl alcohol (IPA)) solution for 10 mins and rinsing with IPA . The functionalized substrate is then covered completely with the CHP GNR dispersion and is incubated for 24 h. Afterwards, the wafer is rinsed with IPA and dried with a nitrogen gun.

GNR dispersion preparation (films): The dispersion is prepared by sonication of GNRs for 30-40 min in a low boiling point organic solvent (*i.e.* THF or CB) and is dropped on the heated substrate immediately after sonication to prevent aggregation of GNR in the solvent.

GNR annealing conditions: The sample is loaded into a furnace with H_2 and Ar flow rates of 15 and 250 sccm respectively. The pressure inside the furnace was set to 6 Torr and the furnace was heated to 500 °C for 2 h.

ATR-FTIR measurement: ATR-FTIR spectroscopy data was obtained using a Bruker Vertex 80v FTIR instrument with a PIKE MIRacle™ ATR unit equipped with a ZnSe crystal. Each sample was placed flush against the surface of the ZnSe crystal to obtain each spectrum. Data was obtained and analyzed using OPUS software with a scan from 500 to 4000 wavenumbers at $2cm^{-1}$ resolution at 32 scans per spectrum. Both the optical bench and sample chamber were under vacuum (2- 5 hPa) for each measurement to remove OH and CO stretching modes from water vapor and carbon dioxide in the atmosphere.

AFM measurement: We used AFM model: Bruker Dimension Icon Scanning Probe Microscope (SPM) with a PeakForce tapping mode. The tip used was Scan Asyst-Air by Bruker with a nominal tip radius of 2 nm and a maximum radius of 12 nm.

Note s2:

Discussion about GNR device study:

Figure s5 shows I-V_d curves of an individual GNR device under gate biases of -50 V, 10 V and, 50 V. Very little gate dependence was observed, which prevented the determination of the electrical bandgap and the mobility. We attribute the absence of gate dependence in these devices to the screening of gate electric field by the closely spaced source and drain electrodes, as SiO_2 thickness is 300 nm while the channel length (or source-drain spacing) is ~ 20 nm. Fabrication of devices with much thinner dielectric is currently ongoing, and the results will be published in a separate paper.

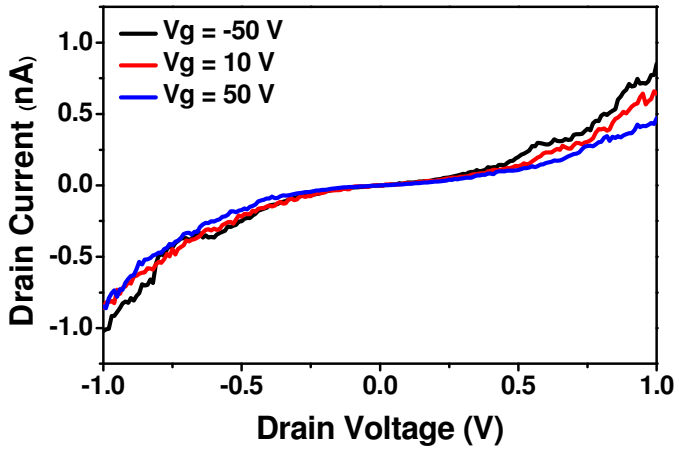

Figure s5. I-V_d curves of an individual GNR device at different gate biases. The weak P-type gate modulation is attributed to the electric field screening effect by the closely positioned source-drain.

Moreover, any twists in the GNR structure will potentially influence the electrical properties of these GNRs as it will locally alter the energy bands and/or create insulating states at the twist location. Therefore, the fabrication of short channel devices (i.e. ~ 20 nm) is important to minimize the probability of twists or other structural defects within the channel.

Although the GNR is semiconducting, the limited p-type current modulation in the GNR films may be attributed to an electric field screening effect in thick (i.e. 30-100 nm) GNR films and relatively high ribbon-to-ribbon junction resistance. When the GNR film is much thicker than the electric field screening length (*i.e.* Debye length), the electric field cannot effectively modulate the charge carriers in the part of the channel that is farthest from the dielectric/channel interface and accordingly the device cannot be completely switched off. Moreover, poor contact between GNRs and/or twists along the length of GNRs can alter the energy band locally which makes the current modulation along the channel less effective and results in poor ON/OFF ratio.

Note s3:

Discussion about GNR film sensing:

We attribute this enhanced NO_2 sensitivity to the semiconducting nature of chemically synthesized GNRs which allows higher level of current modulation *via* adsorption of NO_2 molecules than semimetal pristine graphene. Additionally, compared to graphene, edges of GNRs are more chemically active than pristine Sp^2 surface of graphene which might play an important role in the molecular adsorption and sensing mechanisms. In the future, it may be beneficial to study the sensing performance of GNRs of different width and length to understand the mechanisms behind the high sensitivity of GNR NO_2 sensors.

Figure s6 shows the I-V_d curves of a device before annealing, and after annealing at 300 °C, 400 °C, and 500 °C. It can be clearly seen that annealing at higher temperatures led to higher conduction; however, we found that devices annealed at 300 °C and 400 °C showed unstable conduction and therefore were not used for sensing experiments.

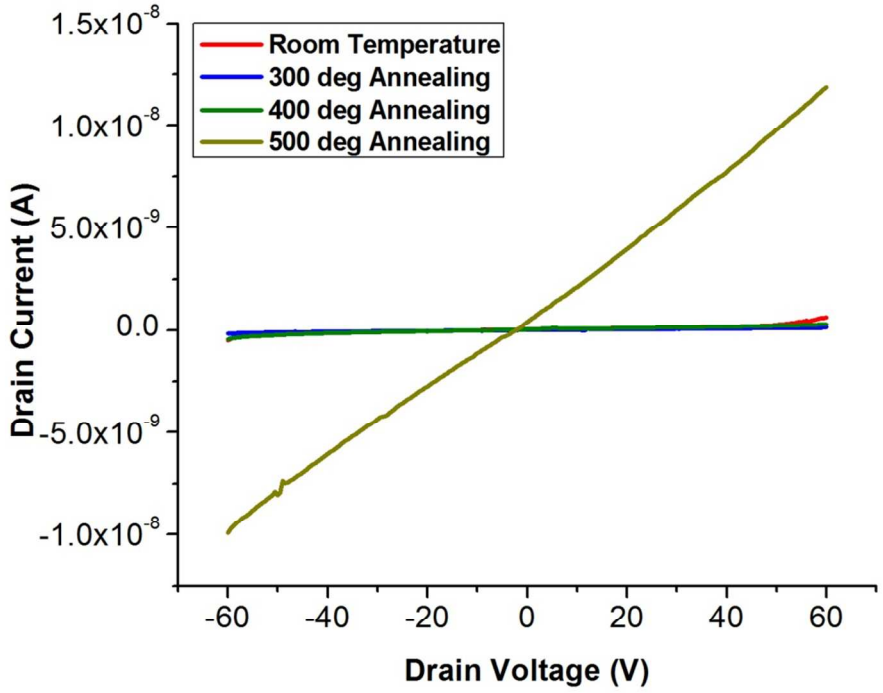

Figure s6. I-V_d curves of a device before annealing, and after annealing at 300 °C, 400 °C, and 500 °C showing significant enhancement in conduction after annealing at 500 °C.

We attribute the response time presented in Figure 4 to the diffusion of NO_2 molecules in Ar and attachment of NO_2 to GNRs, for the rather low concentrations we used. Our response time is comparable to what has been reported in literature, such as exfoliated graphene sensors (Nature Materials, 6, 652-655, **2007**) and In_2O_3 sensors (Nanoletters, 4, 1919-1924, **2004**). We attribute the relatively small conductance change to the low NO_2 concentrations we used.